land

MDPI

Article

Prediction of Soil Erodibility by Diffuse Reflectance Spectroscopy in a Neotropical Dry Forest Biome

Samuel Ferreira Pontes [1], Yuri Jacques Agra Bezerra da Silva [1], Vanessa Martins [2], Cácio Luiz Boechat [1], Ademir Sérgio Ferreira Araújo [3], Jussara Silva Dantas [4], Ozeas S. Costa, Jr. [5] and Ronny Sobreira Barbosa [1,*]

[1] Campus Professora Cinobelina Elvas, Universidade Federal do Piauí, km 01, Rua Manoel Gracindo, Planalto Horizonte, Bom Jesus 64900-000, Piauí, Brazil
[2] Colégio Técnico de Bom Jesus, Universidade Federal do Piauí, km 01, Rua Manoel Gracindo, Planalto Horizonte, Bom Jesus 64900-000, Piauí, Brazil
[3] Departamento de Engenharia Agrícola e Solos, Centro de Ciências Agrárias, Universidade Federal do Piauí, 3397, R. Dirce Oliveira, Teresina 64048-550, Piauí, Brazil
[4] Centro de Ciências e Tecnologia Agroalimentar, Universidade Federal de Campina Grande, 1770, Rua Jario Vieira Feitosa, Pombal 58840-000, Paraíba, Brazil
[5] School of Earth Sciences, The Ohio State University at Mansfield, 1760 University Drive, Mansfield, OH 44906, USA
* Correspondence: ronny.barbosa@ufpi.edu.br

Abstract: The USLE and the RUSLE are two common erosion prediction models that are used worldwide, and soil erodibility (K-factor) is one parameter used to calculate them. The objectives of this study were to investigate the variability of soil-erodibility factors under different soil-texture classes and evaluate the efficiency of diffuse reflectance spectroscopy (DRS) in the near-infrared range at predicting the USLE and RUSLE K-factors using a partial least squares regression analysis. The study was conducted in Fluvisols in dry tropical forest (the Caatinga). Sampling was undertaken in the first 20 cm of soil at 80 sites distributed 15 m apart on a 70 m × 320 m spatial grid. Results show that the clay fraction is represented mainly by 2:1 phyllosilicates. Soil organic matter content is low (<0.2%), which is typical of tropical dry forests, and this is reflected in the high values of the calculated USLE and RUSLE K-factors. An empirical semivariogram was used to investigate the spatial dependence of both K-factors. Pedometric modeling showed that DRS can be used to predict both USLE (R^2_{adj} = 0.53; RMSE = 8.37 10^{-3} t h MJ^{-1} mm^{-1}) and RUSLE (R^2_{adj} = 0.58; RMSE = 6.78 10^{-3} t h MJ^{-1} mm^{-1}) K-factors.

Keywords: Caatinga; USLE; RUSLE; geostatistics; pedometrics; near infrared

check for updates

Citation: Pontes, S.F.; Silva, Y.J.A.B.d.; Martins, V.; Boechat, C.L.; Araújo, A.S.F.; Dantas, J.S.; Costa, O.S., Jr.; Barbosa, R.S. Prediction of Soil Erodibility by Diffuse Reflectance Spectroscopy in a Neotropical Dry Forest Biome. *Land* **2022**, *11*, 2188. https://doi.org/10.3390/land11122188

Academic Editors: Jay Mar D. Quevedo, Norie Tamura, Yuta Uchiyama and Ryo Kohsaka

Received: 4 November 2022
Accepted: 30 November 2022
Published: 2 December 2022

Publisher's Note: MDPI stays neutral with regard to jurisdictional claims in published maps and institutional affiliations.

Copyright: © 2022 by the authors. Licensee MDPI, Basel, Switzerland. This article is an open access article distributed under the terms and conditions of the Creative Commons Attribution (CC BY) license (https://creativecommons.org/licenses/by/4.0/).

1. Introduction

Soil erosion is the movement and transport of soil by various agents, particularly water, wind, and mass movement. Erosion degrades soil quality and is a major reason for farmland loss in the world [1]. Global rates of soil erosion have been exceeding those of new soil formation by 10- and 20-fold on most continents of the world over the past few decades [2]. This increase in soil erosion is strongly linked with the clearance of natural vegetation for agriculture expansion and the use of farming practices unsuited to the land on which they are practiced. This, combined with climatic variation and extreme weather events, has created ideal conditions for soil erosion [3]. The main climatic factors influencing soil erosion are rainfall (amount, frequency, duration, and intensity) and wind (direction, strength, and frequency of high-intensity winds). Additional key factors include drought intensity and frequency, land-use management, soil type, and topography [4].

Traditionally, soil erosion research has relied on direct measurements in the field using erosion plots under natural erosive rainfall. However, this method requires long-term monitoring, which is tedious, time-consuming, labor intensive, and costly [5,6].

Alternatively, pedometrics has been used to predict soil attributes through mathematical models using available soil data. These pedotransfer functions (PTFs) are predictive functions of soil properties that are difficult to obtain from other easily, routinely, or cheaply measured properties (e.g., soil structure and texture obtained from soil surveys). PTFs add value to the basic soil data by translating them into predictors of other, more-laborious and expensively determined soil properties and fill the gap between the available soil data and other properties that are more useful or required for a particular model or quality assessment [7].

An example of a commonly used pedotransfer function is the soil erodibility factor (K-factor), an input variable for the USLE (universal soil-loss equation) [8] and RUSLE (revised universal soil-loss equation) [9], two erosion prediction models used extensively to estimate rates of soil erosion, especially when data of erosional processes are limited [5,6,10,11]. The USLE and the RUSLE are simple, easy, and quick empirical water-erosion models containing six factors (input variables): soil erodibility (K-factor), soil erosivity due to rainfall runoff (R-factor), slope length (L-factor), slope steepness (S-factor), land cover (C-factor), and land-use practice (P-factor) [8,9]. Soil erodibility (K-factor) is an important parameter for estimating soil loss and implementing soil conservation practices [12], and it is highly affected by physical, hydrological, chemical, mineralogical, and biological properties [13]. Unlike the other input variables of the USLE and RUSLE models, the K-factor cannot be estimated directly from readily available data sources (such as rainfall gauges, topographic maps, or land-use data). The K-factor is the only soil-loss factor that is intrinsic to soil features and, as such, provides a quantitative description of the inherent erodibility of a particular soil [12].

Although the K-factor can be calculated from common soil parameters that usually influence the soil resistance to erosion (such as soil texture and organic matter content [14]); in order to obtain these soil parameters, traditional methods, which are also expensive and time-consuming, are still needed. Because of this, the success of proximal soil-sensing techniques in estimating soil properties using the Vis-NIR-SWIR (visible, near-infrared, and shortwave infrared spectroscopy: 350–2500 nm) and the MIR (mid infrared spectroscopy: 4000–400 cm^{-1}) regions is increasing [15,16]. Some advantages of soil spectroscopy analyses include time efficiency, economic convenience, nondestructive application, and freedom from the use of chemical agents and the production of chemical waste [17–20]. Among the spectroscopic techniques used to determine soil properties, diffuse reflectance spectroscopy (DRS) is a well-established, quantitative method long used in physical and analytical chemistry because atoms and molecules absorb radiation in specific wavelengths and have their own unique spectra [5,21–23]. Soil spectroscopy in Vis-NIR-SWIR and MIR integrates the signals from the soil's minerals, organic matter (OM), and water adsorbed or present in mineral structures [24–26]. The spectra provide a 'fingerprint' of the molecular composition of the soil matrix, and research over the past four decades has shown that when soil's physical, chemical, and biological properties derive from or are associated with the mineral–organic matrix, the spectra of air-dry soil can respond to variation in those properties [27].

The Caatinga is a xeric shrubland and thorn forest, which consists primarily of small, thorny trees that seasonally shed their leaves. Cacti, thick-stemmed plants, thorny brush, and arid-adapted grasses make up the ground layer. Many annual plants grow, flower, and die during the brief rainy season. About 60% of the rainfall occurs in a single month, up to 20% of it occurring in a single day of the year [28]. Average annual temperatures are high (23–27 °C) and relative humidity is usually below 50% [29]. This biome, unique to Brazil, covers an area of 912,529 km^2, accounting for 10.7% of the Brazilian territory, and it is considered the largest seasonally dry tropical forest in the neotropics [30]. It is a diverse biome, encompassing 17 great landscape units, subdivided into 105 geo-environmental units out of a total of 172 for the whole northeast region of Brazil [31]. It has been recognized as the most species-rich neotropical dry forest biome, supporting 950 genera, 3150 species, and 152 families of flowering plants, one-third of which are

endemic to the Caatinga [32]. Within this complex and diverse region lives a population of more than 20 million people, making it one of the most densely populated semiarid regions in the world: 26 inhabitants per km^2 [33].

Although there is significant spatial variability, four dominant soil orders cover about 68% of the biome [29]: *Latosolos* (Ferralsols/Oxisols), which are soils with highly advanced development resulting from intense weathering in the primary minerals, cover about 21% of the Caatinga; *Cambissolos* (Inceptisols), which are poorly developed soils with an incipient B horizon, cover about 19% of the biome; *Argisolos* (Acrisols/Ultisols), which are soils with advanced development and a diagnostic textural B horizon, cover about 15%; *Luvisolos* (Luvisols/Alfisols), which also shows advanced development with iron oxide production and clay mobilization from topsoil, cover about 13% of the biome. According to the same authors, *Neossolos Regolíticos* (Regosols/Entisols), a group of poorly developed soils resulting from the weak action of pedogenetic processes, account for only 4% of the biome's soils. Previous studies have shown that areas of bare *Luvisolos* (Luvisols/Alfisols) and *Argisolos* (Acrisols/Ultisols), which cover over a quarter of the Caatinga, are the most prone to soil erosion. These studies have estimated that the annual soil loss in this biome ranges from 3 to 50 tons ha^{-1} [34,35]. There is also evidence of several hotspots of advanced desertification [36]. Borrelli et al. [37] show that about 6.1% of the global land area experienced very high soil erosion rates (exceeding 10 Mg $ha^{-1}yr^{-1}$) in 2012, particularly in dry regions including South America, Africa, and Asia, which can be leading to desertification. Such facts highlight the relevance of advancing the study of erosion in sandy soils, especially in semiarid tropical regions [38,39].

The main objectives of this study were to (i) investigate the variability of the USLE and RUSLE K-factors under different soil-texture classes; (ii) perform a geostatistical modeling of these K-factors and observe their spatial variability and similarity; and (iii) evaluate the efficiency of the DRS at predicting these K-factors through partial least squares regression analysis (PLSR) under different soil-texture classes.

2. Materials and Methods

2.1. Study Area

The study was conducted in 5.5 acres of mixed cropland (passion fruit) and pastureland in the municipality of São Domingos, state of Paraíba, Brazil, at coordinates 6°48′45″ S and 37°56′12″ W (Figure 1). The local climate is classified as tropical semiarid (BSh) by the Köppen system, with an average annual rainfall of 659 mm (50% of which falls during the months of March and April) and annual average temperatures of 28 °C [40].

Metabasic and metacarbonate rocks (including banded migmatites and gneisses) and alluvial deposits (sand, gravel) characterize the parent material of the study area [41]. The soil in this region is classified as *Neossolo Flúvico Ta Eutrófico* (RYve), which has high activity clay and a base saturation of $\geq$ 50%, according to the Brazilian Soil Classification System [42], which is equivalent to Fluvisols [43] and Entisols [44]. This soil is derived from medium-grained arcosian sandstones deposited in a Holocene alluvial plain [41]. The relief is flat to gently wavy, with altitudes ranging from 183 to 193 m. About 37% of the study area contain slopes with 4–12% inclination and 20% with slopes steeper than 12%, resulting in high erosion risks in cultivated areas [45].

2.2. Soil Sampling and Analysis

Sampling was undertaken in the first 20 cm of soil using a stainless-steel auger, in a sampling grid with 80 points spaced 15 m apart (Figure 1). The location of each sampling point was georeferenced using a Garmim® GPS, etrex model. Soil samples were air-dried and sieved through a 2 mm mesh nylon sieve. The pipette method was used to determine grain size, using a 1 mol L^{-1} sodium hydroxide solution as a dispersant agent [46]. Sieving was used to subdivide the sand fraction into very coarse sand (VCS, 2–1 mm), coarse sand (CS, 1–0.5 mm), medium sand (MS, 0.5–0.21 mm), fine sand (FS, 0.21–0.105 mm), and very fine sand (VFS, 0.105–0.053 mm), according to the international standard for soil

classification provided by the International Union of Soil Sciences [43]. The quantification of clay dispersed in water (CDW), to determine its natural flocculation degree, was obtained following the procedure in [46]. The determination of SOM was conducted following the methodology described by Raij and collaborators [47]. The same procedures described above were adopted by [48].

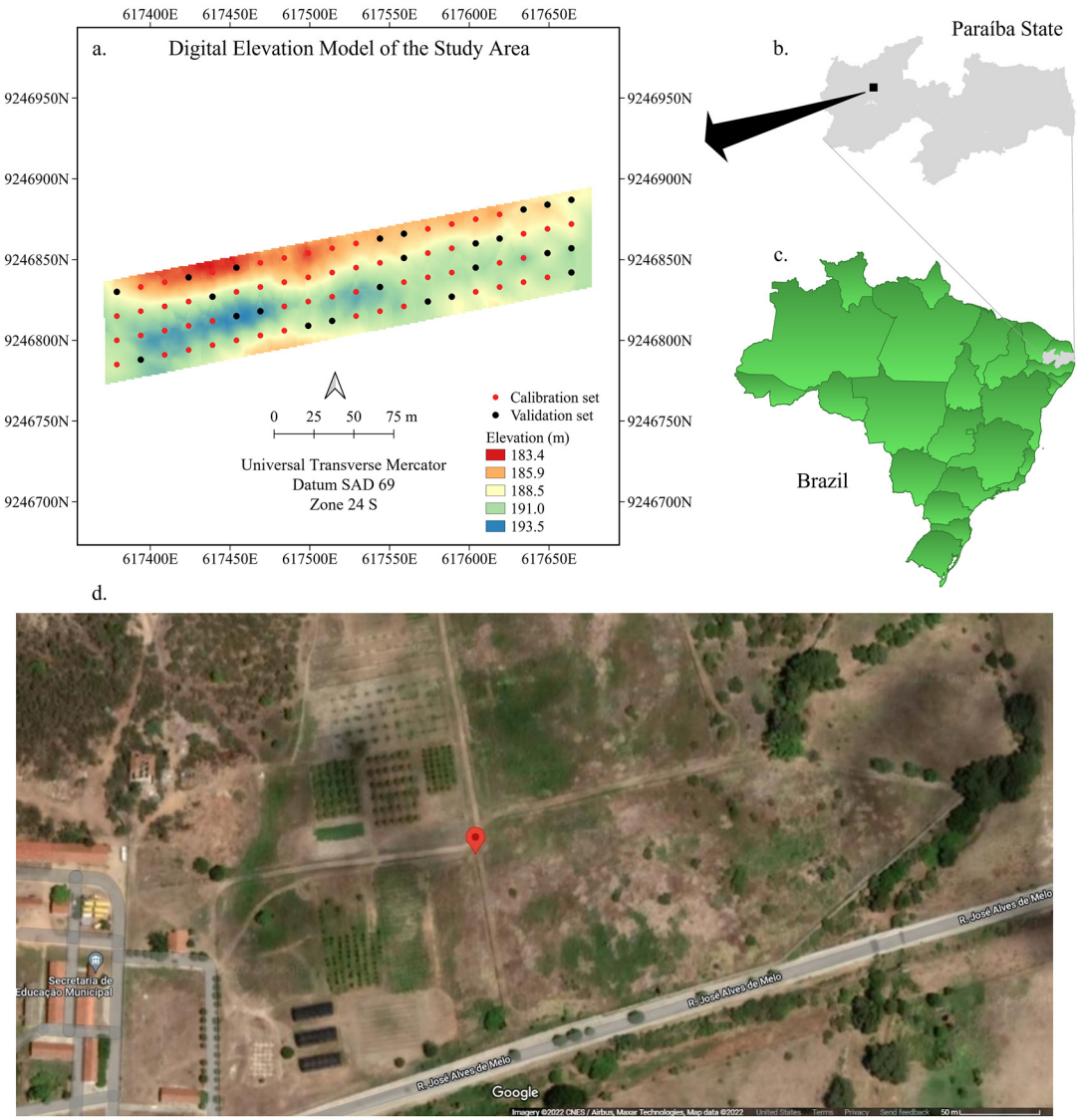


Figure 1. Geographical location of the study area. (**a**) Digital elevation model of the study area and location of the soil samples. (**b**) State of Paraíba. (**c**) Brazil. (**d**) Satellite image of the study area with the entrance indicated as red icon.

2.3. Calculation of Erodibility Factors

The erodibility factor (K-factor) is computed as the rate of soil loss per unit of rainfall erosion index as measured on a unit plot. Because obtaining a direct measurement of the K-factor is costly, time-consuming, invasive, and method dependent, pedotransfer functions (PTF) have been widely used to predict K-factor using easily measurable basic soil properties [49]. The following models were used to obtain the values of the erodibility factors:

(a) USLE K-factor, calculated according to the equation proposed by Denardin [50]:

$$\text{USLE K-factor} = 0.00000748 \times \text{M} + 0.00448059 \times \text{P} - 0.0631175 \times \text{MWD} + 0.01039567 \times \text{REL} \quad (1)$$

where M = (%silt + %VSF) × (100 − %clay), P = permeability code coded according to Wischmeier and collaborators [51] (dimensionless), MWD = mean weight diameter of soil particles lower than 2 mm, and REL = %SOM ÷ % ≥ 0.1 mm (dimensionless).

(b) RUSLE K-factor, calculated according to the equation proposed by Renard and collaborators [9]:

$$\text{RUSLE K-factor} = 0.0034 + 0.0405 \exp\left[-0.5\left(\frac{\log D_g + 1.659}{0.7101}\right)^2\right] \quad (2)$$

$$D_g = \exp[\sum 0.01 f_i \ln\{(d_{max} + d_{min})/2\}] \quad (3)$$

where D_g represents geometric mean particle size (for clay, silt, and sand), d_{max} represents maximum diameter (mm), d_{min} represents minimum diameter, and fi represents the corresponding fraction of mass.

2.4. Diffuse Reflectance Spectroscopy

Air-dried soil samples were ground in an agate mortar to a particle size smaller than 2 mm and placed into a 10 mm diameter Petri dish. They were then oven-dried at 40 °C for 24 h, after which the spectrum was recorded for each sample by using a Fourier transform infrared spectrometer (FTIR Spectrum Frontier MID NIR—Perkin Elmer) in the near-infrared range (NIR) (1000–2500 nm; 10,000–4000 cm^{-1}) at 0.5 nm intervals (Figure 2). Each sample was scanned four times with the Petri dish in different positions, to ensure that the maximum sample area was represented. The spectrum for each sample is the average of the four recordings. The fluoropolymer Spectralon (nominal reflectance of 99%) was used as a white diffuse reflectance standard. The spectra were then subjected to standard normal variate (SNV) preprocessing to minimize secondary effects. SNV preprocessing consists of subtracting each spectrum by its own mean and dividing it by its own standard deviation [52,53].

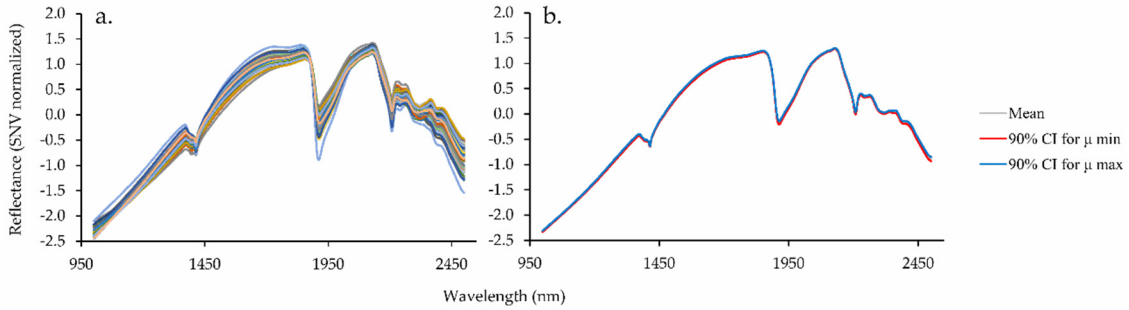


Figure 2. The raw spectral reflectance data of the soil samples of the studied site after normalization by the standard normal variate (SNV) method (n = 80). Each line represent one sample. (**a**) and the mean spectra with its 90% confidence interval (**b**).

2.5. Data Analysis

A descriptive statistical analysis was conducted on all studied variables, including the calculation of the standard deviation (SD) and coefficient of variation (CV). A one-way analysis of variance (ANOVA) was used for the investigation of the effects of soil-texture classes on the USLE and RUSLE K-factors where Tukey's test was conducted. The descriptive statistical analysis and ANOVA were conducted on Minitab software (version 19).

Geostatistical analyses were used to analyze and predict the values associated with the spatial distribution of soil properties [54]. The semivariance ($\hat{\gamma}$), which measures dissimilarity between values sampled at sites separated by a distance h, was calculated

to develop experimental semivariograms (spherical, exponential, or Gaussian), using the following equation:

$$\hat{\gamma}(h) = \frac{1}{2N(h)} \sum_{i=1}^{N(h)} [Z(x_i) - Z(x_i + h)]^2 \quad (4)$$

where N(h) is the number of pairs of measured values separated by the distance h and Z is the value measured in the points x_i and x_i + h.

This modeling allowed the determination of the following geostatistical parameters: the nugget effect (C_0), the sill (C_0 + C_1), the range (a), and the degree of spatial dependence {DSD [(C_0/C_0 + C_1)]}. We also conducted an evaluation of spatial dependence (ESD) [55], where strong dependence (S), medium dependence (M), and weak dependence (W) corresponded to DSD $\leq$ 0.25, DSD $\leq$ 0.75 and >0.25, and DSD > 0.75, respectively. The performance of the experimental semivariograms was evaluated by examining the coefficient of determination (R^2) and the root mean squared error (RMSE) for the modeled parameters. The ordinary kriging method was used for the spatial interpolation of the measured/calculated parameters. The RMSE was calculated using the following equation:

$$RMSE = \sqrt{\frac{\sum_{i=1}^{n} (P_i - O_i)^2}{n}} \quad (5)$$

where Σ means "sum", P_i represents the predicted value for the ith observation in the data set, O_i is the observed value for the ith observation in the data set, and n is the sample size. The geostatistical modeling was conducted in QGIS software (version 3.10), using the complement Smart-Map.

Prediction Model Testing

For pedometric analysis and modeling, the data were divided into two sets: a calibration set and a validation set. The calibration set was composed of 56 samples (70%), while the validation set was composed by 24 samples (30%) (Figure 1). Calibration was conducted using a partial least squares regression analysis (PLSR) [56] in ParLeS® software [57]. The number of predictive variables for the application of PLSR was determined using a leave-one-out cross-validation method with the purpose of determining the number of factors (F) to be retained in the validation models [58]. The selection of F was conducted following the smaller number of Akaike information criterion (AIC) for each prediction [59]. The validation of these predictive models was conducted by external validation, using the validation set by linear regression. Different authors have been using PLSR in pedometric modeling when the predictive attributes were obtained by DRS [60–64].

The efficiency of the predictive models was assessed by the adjusted determination coefficient (R^2_{adj}), the RMSE, and the residual prediction deviation (RPD), which is calculated using the following equation:

$$RPD = \frac{SD}{RMSE} \quad (6)$$

where SD is the standard deviation of the original data and RMSE is the root mean squared error of validation.

For RPD values, we considered [65]: RPD < 1 indicates not very reliable predictions, RPD ranging from 1.4 to 2 indicates reliable predictions, and RPD > 2 indicates good predictions. In this study, we considered as 'reliable to pass for external validation' only those models that presented RPD $\geq$ 1.4. The importance of a variable in the prediction of another was given by the index of variable importance in the projection (VIP), where variables that better predict the attributes have higher peaks in the VIP graph [66].

3. Results

3.1. Soil-Texture Distribution

The grain size distribution of the soil samples is provided in Table 1. The mean concentration of the granulometric fractions decreased in the following order: sand > silt > clay,

where the sand fraction showed the widest range (206 to 942 g kg^{-1}). Very fine sand (VFS), the sand fraction with the highest mean concentration (240.28 g kg^{-1}), also presented the smallest variability (SD = 62.79 g kg^{-1}). Conversely, the sand fraction with the highest texture variability within the study area belongs to the fine sand (FS) class (mean = 236.10 g kg^{-1}; SD = 102.90 g kg^{-1}).

Table 1. Descriptive statistics of soil properties (n = 80).

Soil Properties	Range	Mean	Median	SD	CV
Clay (g kg^{-1})	34.51–312.89	109.81	100.00	59.77	54.43
Silt (g kg^{-1})	20.00–575.03	239.00	245.50	122.1	51.08
Sand (g kg^{-1})	206.01–942.00	651.10	650.50	177.00	27.19
VCS (g kg^{-1})	5.00–77.01	27.47	25.00	12.17	44.29
CS (g kg^{-1})	6.00–202.10	42.68	37.00	30.17	70.69
MS (g kg^{-1})	11.02–496.00	104.65	94.30	74.63	71.31
FS (g kg^{-1})	43.10–508.00	236.10	232.50	102.90	43.58
VFS (g kg^{-1})	41.03–384.00	240.28	253.00	62.79	26.13
CDW (g kg^{-1})	5.51–158.20	65.02	59.00	31.98	49.19
SOM (dag kg^{-1})	0.01–0.25	0.10	0.10	0.05	51.86
USLE K-factor (10^{-3} t h MJ^{-1} mm^{-1})	0.07–45.56	29.01	30.57	9.22	31.77
RUSLE K-factor (10^{-3} t h MJ^{-1} mm^{-1})	7.52–43.83	20.89	19.71	10.31	49.35

SD, standard deviation; CV, coefficient of variation (%); VCS, very coarse sand; CS, coarse sand; MS, medium sand; FS, fine sand; VFS, very fine sand; CDW, clay dispersive in water; SOM, soil organic matter, USLE K-factor, the soil erodibility factor of the universal soil-loss equation (USLE) calculated according to Denardin [49]; and USLE K-factor, the soil erodibility factor of the revised universal soil-loss equation (RUSLE) calculated according to Renard et al. [9].

The CDW content did not exceed 16% and presented CV near 50%. The SOM content was low and did not exceed 0.2%. Although both USLE and RUSLE models similarly produced the highest erodibility factors (USLE K-factor: 45.56 × 10^{-3} t h MJ^{-1} mm^{-1}; RUSLE K-factor: 43.83 × 10^{-3} t h MJ^{-1} mm^{-1}), the lowest USLE K-factor value is over 107 times smaller than the lowest calculated RUSLE K-factor.

The soil type varies from loamy to sandy soils, with clay content ranging from 3% to 31%, silt content from 2% to 57%, and sand content from 21% to 92%. Most samples (41%) are classified as sandy loam; another 31% of samples are classified as loamy sand; and another 19% are classified as loam (Figure 3).

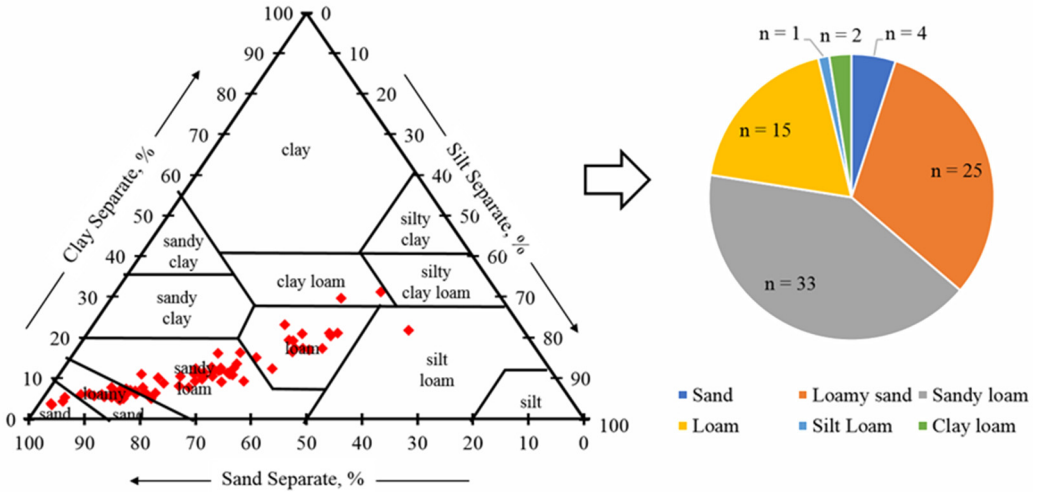


Figure 3. The soil-texture distribution of the study area, according to the international standard for soil classification provided by the International Union of Soil Sciences. The red rhombuses mean the soil samples.

3.2. K-Factor Distribution

Figure 4 shows individual value plots for the USLE and RUSLE K-factors by different soil-texture classes, compared by Tukey's test. For the USLE K-factor, there is no significant statistical difference between the clay loam and the silt loam, loam and sandy loam. However, they were statistically different from loamy sand and sand. For the RUSLE K-factor, clay loam and silt loam, loam, sandy loam and loamy sand are statistically different, whereas there is no significant statistical difference between loamy sand and sand. In other words, the mean of USLE K-factor by soil texture follows: clay loam and silt loam = loam = sandy loam > loamy sand > sand. On the other hand, the mean of RUSLE K-factor by soil texture follows: clay loam and silt loam > loam > sandy loam > loamy sand = sand.

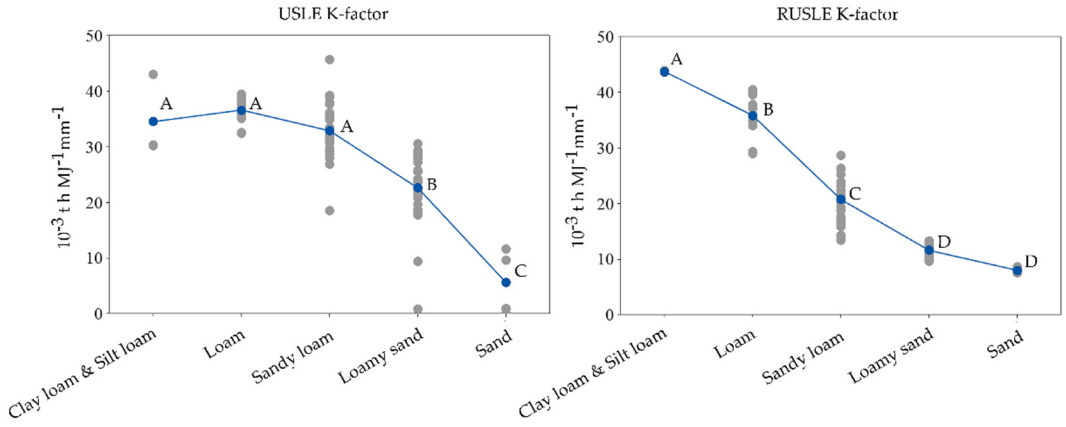


Figure 4. The individual value plots of the K-factors of the USLE and RUSLE models under different soil-texture classes from the study area. The gray dots represent the individual values, and the blue dots represent the mean. Same letter indicates the difference between the means is not statistically significant according to Tukey's test.

3.3. Geostatistical (Spatial) Modeling

The model parameters adjusted to the data of semivariograms are presented in Table 2. The experimental models that presented better fit for most attributes were the spherical semivariogram model (clay, sand, CS, MS, and RUSLE K-factor), followed by the exponential semivariogram model (silt and USLE K-factor). For measured FS content, the most adequate model was the Gaussian semivariogram model. All variables showed medium spatial dependence, except silt, which presented strong spatial dependence. The range fluctuated from 34 m (CS) to 140 m (FS and USLE K-factor). Most attributes presented R^2 higher than 0.70, indicating positive fit to the semivariograma, except for MS and CS. The USLE K-factor and RUSLE K-factor showed R^2 equal to 0.83 and 0.80, respectively. The parameters VFS, CDW, and SOM did not fit a semivariogram, because of the occurrence of pure nugget effect (PPE), suggesting total absence of spatial autocorrelation in these parameters.

Figure 5 displays the thematic maps for each parameter adjusted to the data of semivariograms presented above. Clay content and silt content are inversely proportional to sand content, the FS map showing higher similarity to the sand map. As for the maps of USLE K-factor and RUSLE K-factor, there is a clear, strong correlation between soil erodibility and sand content, particularly in the RUSLE model.

3.4. Spectral Signature and Pedometrics

Figure 6 shows the changes in spectral reflectance of the data from different soil-texture classes after normalization by the standard normal variate (SNV) method. The line colors correspond to the different soil-texture classes. The figure shows the presence of representative peaks in the wavelength near to 1350 and 2125 nm, as well as representative valleys in the wavelength near to 1400, 1900, and 2200 nm. In addition, each soil-texture

class presents a distinct pattern of spectral signatures in different wavelengths. For instance, the peak/valley combination observed at 1350 nm and 1400 nm (Figure 6, inset 1) shows the reflectance decreasing in the following order: clay loam + silt loam > loam > sandy loam > loamy sand > sand. Conversely, for the valleys observed at 1900 nm (Figure 6, inset 2) and at 2200 nm (Figure 6, inset 4), as well as the peak observed at 2125 nm (Figure 6, inset 3), the reflectance decreases in the following order: sand > loamy sand > sandy loam > loam > clay loam + silt loam.

Table 2. Estimated model and parameters of the semivariograms of the soil properties.

Soil Properties	Model	C_0	$C_0 + C_1$	DSD	ESD	a (m)	R^2	RMSE
Clay (g kg^{-1})	Sph	8	27	0.28	M	70	0.77	43
Silt (g kg^{-1})	Exp	37	167	0.22	S	134	0.93	404
Sand (g kg^{-1})	Sph	88	344	0.26	M	75	0.82	5887
VCS (g kg^{-1})	PPE	-	-	-	-	-	-	-
CS (g kg^{-1})	Sph	1	4	0.26	M	34	0.21	2
MS (g kg^{-1})	Sph	10	26	0.39	M	55	0.59	46
FS (g kg^{-1})	Gau	57	128	0.44	M	140	0.96	171
VFS (g kg^{-1})	PPE	-	-	-	-	-	-	-
CDW (g kg^{-1})	PPE	-	-	-	-	-	-	-
SOM (dag kg^{-1})	PPE	-	-	-	-	-	-	-
USLE K-factor (10^{-3} t h MJ^{-1} mm^{-1})	Exp	21	60	0.35	M	140	0.83	115
RUSLE K-factor (10^{-3} t h MJ^{-1} mm^{-1})	Sph	32	116	0.28	M	72	0.80	685

Sph, spherical; exp, exponential; PPE, pure nugget effect; Gau, Gaussian; C_0, nugget effect; $C_0 + C_1$, still; DSD [$(C_0/C_0 + C_1)$], degree of spatial dependence; ESD, evaluation of spatial dependence assessment; S, strong dependence; M, medium dependence; a, range; R^2, determination coefficient; and RMSE, root mean squared error.

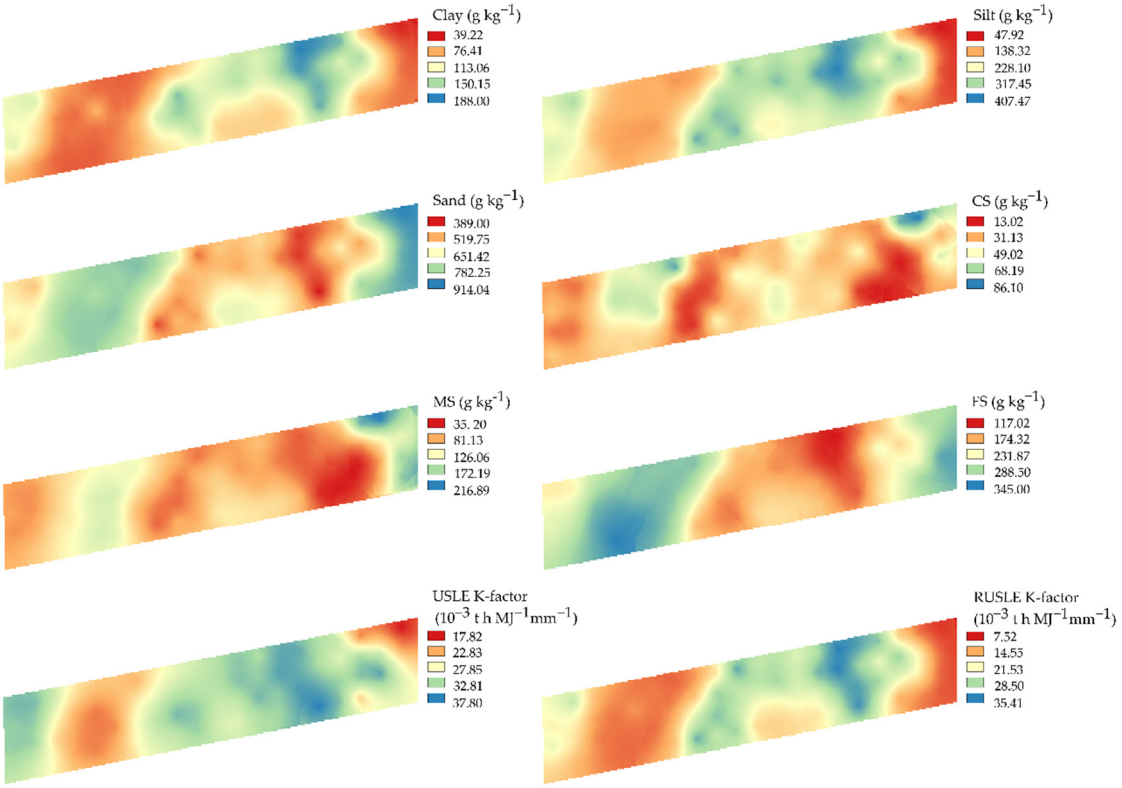


Figure 5. Spatial distribution maps of soil properties that showed spatial variability.

Table 3 presents the summary of results obtained through PLSR by cross validation and parameters of external validation of the studied soil properties. The F used for the pedometric modeling ranged from 2 to 7. The soil parameters that showed $R^2_{adj} > 0.5$

were the same that presented RPD > 1.4, meaning that they were subjected to the external validation. Furthermore, the values of both R^2_{adj} and RPD decreased in the following order: sand > RUSLE K-factor > clay > silt > USLE K-factor > SOM > CDW > FS. After external validation, FS showed parameters that do not allow the recommendation of its prediction by DRS in the NIR. All others presented good parameters of external validation, including the USLE- and RUSLE-modeled erodibility factors. The USLE K-factor expressed R^2_{adj} of 0.53 and RMSE of 8.37 10^{-3} t h MJ^{-1} mm^{-1}, whereas the RUSLE K-factor showed R^2_{adj} of 0.58 and RMSE of 6.78 10^{-3} t h MJ^{-1} mm^{-1}. Soil parameters VCS, CS, MS, and VFS were not validated, because they did not show enough potential for prediction by DRS in the NIR, because they presented RPD ranging from 1.0 to 1.1.

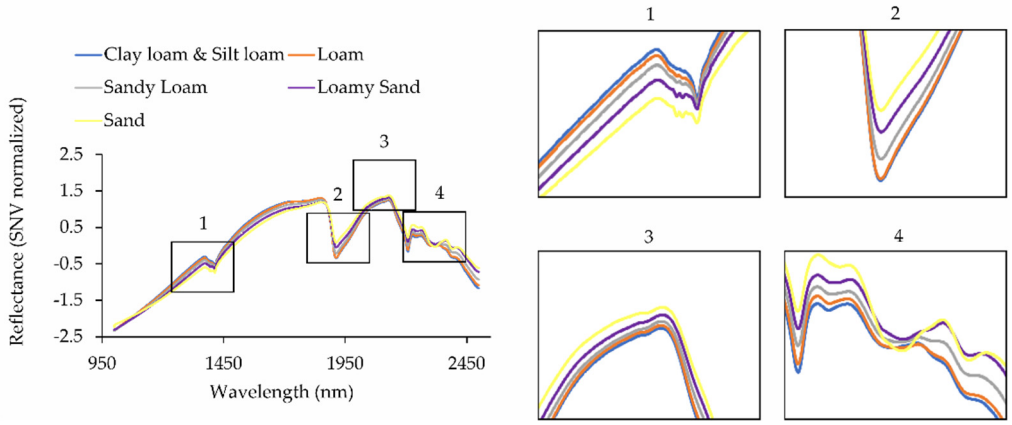


Figure 6. Changes in spectral reflectance of the data from different soil-texture classes after normalization by standard normal variate (SNV) method. Each color represents the average of the correspondent class.

Table 3. Summary of results obtained through PLSR by cross validation and parameters of the external validation of the studied soil properties.

Soil Properties	Parameters of Calibration n = 56						Parameters of External Validation n = 24			
	F	R^2_{adj}	a	b	RMSE	RPD	R^2_{adj}	a	b	RMSE
Clay (g kg^{-1})	4	0.79	0.81	2.19	2.91	2.2	0.57	1.14	0.09	4.09
Silt (g kg^{-1})	6	0.79	0.84	4.23	5.60	2.2	0.66	1.10	0.02	8.50
Sand (g kg^{-1})	6	0.82	0.85	9.53	7.67	2.4	0.68	1.10	−10.10	11.09
VCS (g kg^{-1})	2	0.01	−0.02	2.60	1.04	1.0	-	-	-	-
CS (g kg^{-1})	2	0.06	0.10	3.38	2.08	1.0	-	-	-	-
MS (g kg^{-1})	2	0.19	0.23	7.14	6.04	1.1	-	-	-	-
FS (g kg^{-1})	6	0.62	0.71	6.79	6.51	1.6	0.28	0.54	11.70	8.85
VFS (g kg^{-1})	2	0.13	0.17	20.20	5.45	1.1	-	-	-	-
CDW (g kg^{-1})	4	0.67	0.70	2.14	1.89	1.8	0.57	0.79	2.12	2.09
SOM (dag kg^{-1})	5	0.68	0.73	0.03	0.03	1.8	0.74	0.99	0.01	0.03
USLE K-factor (10^{-3} t h MJ^{-1} mm^{-1})	7	0.70	0.76	7.53	3.75	1.8	0.53	0.64	12.10	8.37
RUSLE K-factor (10^{-3} t h MJ^{-1} mm^{-1})	5	0.81	0.83	3.73	4.67	2.3	0.58	0.98	2.86	6.78

F, number of PLSR factors used in the model; R^2_{adj} = adjusted determination coefficient; SDE, standard deviation of the distribution error; RPD, residual prediction deviation; a, slope; b, intercept.

The VIP plots (Figure 7) provide a better separation of the wavelengths highlighted in Figure 6 that influence soil attribute prediction. The valley observed at 1900 nm is a more representative VIP for clay, silt, sand, CDW, and RUSLE K-factor, while the more relevant VIP for SOM and USLE K-factor matches the valley observed at 2200 nm.

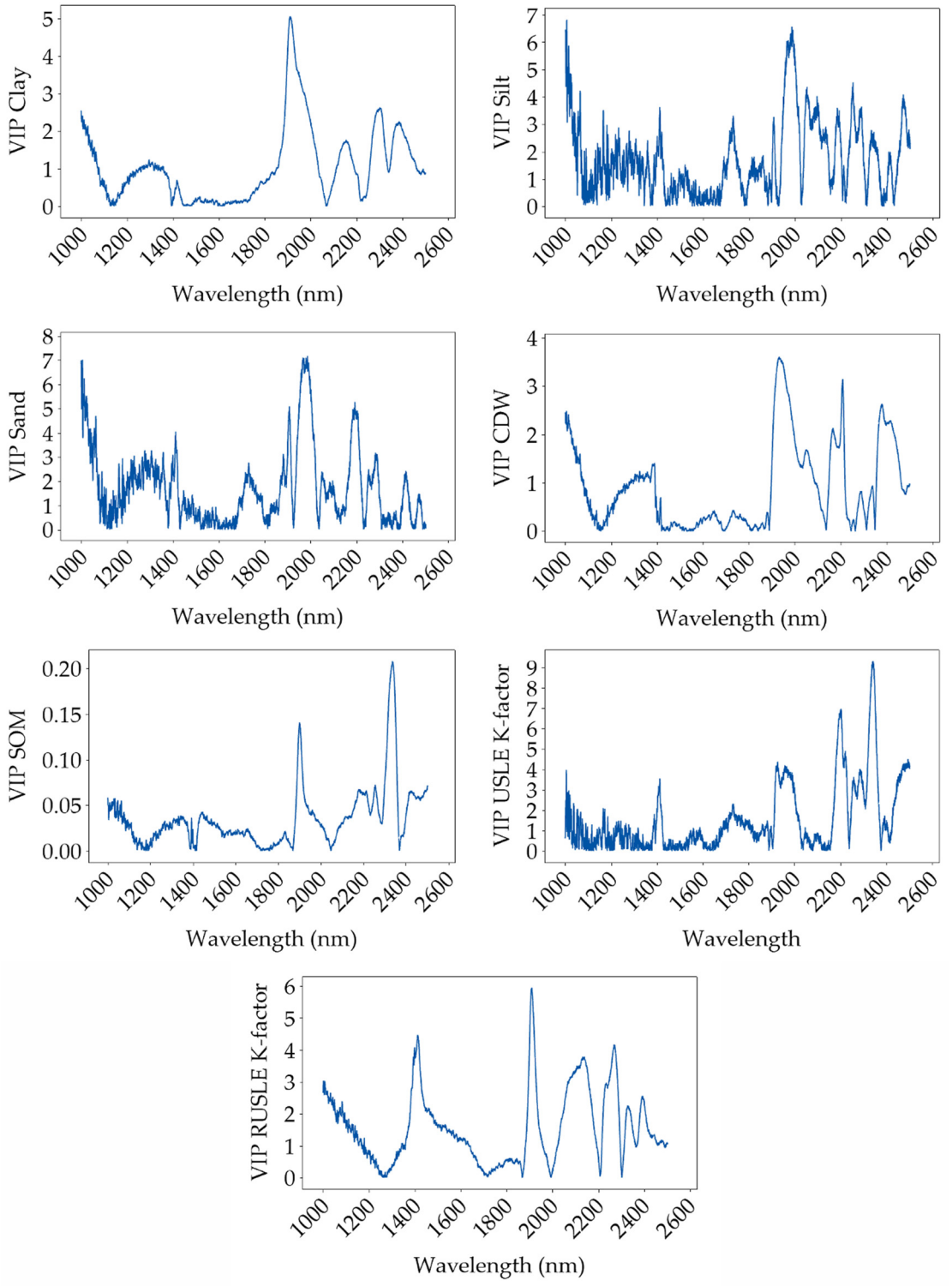


Figure 7. Variable importance for projection (VIP) plots of the studied attributes.

4. Discussion

4.1. Soil Characteristics and Susceptibility to Erosion

The soil-formation processes active in the Caatinga, in particular the low availability of water to hydrolyze primary minerals from parent materials into clay minerals, result in the dominance of the sand fraction [30], which, in our study area, represents about 65% of the soil content. These soils are dominated by sandy loam and coarser textures, similar to what has been observed elsewhere in the Caatinga biome [67–69]. This textural

distribution is likely an outcome of the nature of the parent material given that variations in the proportions of the various particle sizes in a given soil are strongly influenced by the geochemistry of the parent rock [70,71]. Unsurprisingly, the soils in the study area, which are derived from arcosian sandy sediments deposited during the Holocene, have high silica content. This recent depositional history of the study area also accounts for the heterogeneity and observed spatial variability in soil texture, resulting in a mosaic of geomorphic domains, as described previously [41].

It is well established that grain size is an important factor influencing soil erodibility in arid and semiarid regions. A soil-erodibility study in the Middle East showed that sand content has a strong negative correlation with soil erodibility, while silt content had the highest positive correlation [72]. These authors observed that silt and fine sand particles are highly susceptible to soil detachment and transport. Others have observed similar relationships in semiarid regions of Europe [73] and Asia [74]. In our study area, the high concentration of fine (FS) and very fine sand (VFS) suggests that these soils are susceptible to significantly high levels of detachment and transport.

Another important factor influencing soil erodibility is the soil organic matter (SOM) content [5,75–77]. These studies have shown a strong negative correlation between SOM content and soil erodibility, owing to OM's ability to act as a particle aggregator, improving soil stability and significantly reducing soil detachment and transport. Typical undisturbed Caatinga soils have SOM content varying from 0.23% to 1.53% [69]. Our results show that SOM concentrations in the study area are near the minimum value proposed by these authors. This may be explained by the soil management in the area (low-intensity polyculture and pasture), combined with the coarse soil texture and the dry, arid climate conditions. The ongoing passion fruit cultivation in the study area likely does not provide enough organic material to increase SOM or to replace the OM lost by the removal of native vegetation. In addition, the dominant coarse texture in the study area (sandy loam and coarser) has been negatively correlated with whole soil organic content [78,79]. Furthermore, other studies suggest that the predominance of sand fraction in the soil leads to significant oxidation of SOM, which is potentialized in warmer climates [80,81]. This inverse correlation between sand content and SOM has been reported not only in arid regions but also in humid climates [82].

4.2. Factors Affecting Soil Erodibility in the Study Area

In addition to soil properties (e.g., texture, structure, OM content, and aggregate stability), several other factors affect the inherent susceptibility of soils to erosion. These include rainfall intensity [83], slope [84], and land-use practices [85]. In our study area, rainfall-induced soil erosion risk is particularly high during the short but intense rainy season, the months of March and April receiving 50% of the annual precipitation. Both rill and interrill erosion rates are high, with rainfall events greater than 51 mm representing only about 15% of all rain events but concentrating over 36% of the total precipitation [86].

Regarding the slope effect on erosion rates, a number of simulated rainfall studies have explored the combined effects of slope angle and rainfall intensity on soil erosion, although only a few have taken place in arid regions [87–89]. These studies have found that the hydraulic conditions of overland flow (e.g., flow velocity and resistance) determine the erosive forces acting on the soil surface. Thus, on steep slopes (>16% gradient), much of the soil loss is dominated by rill erosion, while interrill erosion is more prominent in gentle slopes (<9% gradient). About 37% of our study area contains slopes with 4–12% inclination and 20% with slopes steeper than 12%.

As for land-use practices, because of the harsh climate and low soil fertility, agricultural fields traditionally occupied only about 10% of the whole semiarid region [90], with less than 2% being permanent crops, and 80% of farms being smaller than 10 ha in size [91]. Over the past two decades, irrigation and high-input agriculture have significantly expanded in the Caatinga [92]. Today, agricultural and agroforestry systems utilize 28.7% of the biome area, totaling 1.9 million properties, of which 31% are larger than 10 ha [93]. The same data

set shows that another 38.7% of the biome area is used as pasture for livestock production. Habitat loss and deforestation from the combined expansion of both crop production and livestock production, which are projected to increase by about 40% over the next decade, constitute the largest threat to the Caatinga [92]. In addition, only about 1% of the biome is under strict legal protection [94].

Various pedotransfer functions have input variables that consider the combined impacts of rainfall, slope, and land use in its prediction of soil loss from erosion [49]. In the case of the USLE and RUSLE soil-loss equations, as indicated previously, these input variables are the R-factor (rainfall-runoff erosivity factor), the L-factor (slope-length factor), the S-factor (slope-steepness factor), the C-factor (cover-management factor), and the P-factor (support-practice factor). Another input variable used in these pedotransfer functions is the K-factor (soil-erodibility factor), which is highly affected by physical, hydrological, chemical, mineralogical, and biological properties and therefore cannot be estimated directly from readily available data sources (such as rainfall gauges, topographic maps, or land-use data). The K-factor is the only soil-loss factor that is intrinsic to soil features and, as such, provides a quantitative description of the inherent erodibility of a particular soil [12]. Coarse-textured soils, such as the sandy soils in our study area, have low K-values (usually below 0.05 t h MJ^{-1} mm^{-1}), mostly because they produce low rates of runoff, even though these soils are easily detached. The mean K-factors calculated in this study (USLE: 0.029 t h MJ^{-1} mm^{-1}; RUSLE: 0.021 t h MJ^{-1} mm^{-1}) are in agreement with those reported from semiarid regions in Africa (0.025 t h MJ^{-1} mm^{-1} [95]), Asia (0.030 t h ha MJ^{-1} mm^{-1} [72]), Europe (0.032 t h ha MJ^{-1} mm^{-1} [96]), and South America (0.039 t h MJ^{-1} mm^{-1} by [97]). These authors have found significant correlations between their predicted K-values and those derived from unit plots measurements.

4.3. Spatial Distribution of Modeled Parameters

Geostatistical modeling was conducted to characterize (model) the spatial autocorrelation of the measured parameters (via a semivariogram) and to create continuous maps based on their spatial distribution (using kriging interpolation). The results of the analysis revealed that both K-factors have strong spatial dependence, as observed elsewhere [55]. Spatial dependence is the property of random pairs of variables (located a certain distance apart) taking values that are more similar (positive autocorrelation) or less similar (negative autocorrelation). The results of our geostatistical analysis clearly show that our data set has a high degree of spatial dependence (i.e., high positive spatial autocorrelation), which is a precondition for the representation of the data on continuous maps. The resulting spatial distribution of the USLE K-factor was best fitted to the exponential model, whereas the RUSLE K-factor was best fitted to the spherical model, along with most of the soil variables. As observed by [48,52], the spherical model is usually more efficient at adjusting experimental semivariograms for the majority of soil attributes. The lack of spatial dependence on a few soil variables, such as SOM, may be explained by the difficulty of modeling semivariograms for attributes that have very small concentrations [98]. Nevertheless, the strong correlation between the K-factors and the grain size suggests that this parameter can be, in the absence of SOM, a strong predictor of soil erodibility in the Caatinga, which is consistent with observations made elsewhere [13,97,99].

The range of the spatial dependence of the K-factors was similar to that of other soil variables, which also showed spatial dependence [55] and showed that distance was higher than the spacing between sampled points (15 m). As indicated above, the fact that a positive spatial autocorrelation exists between the sampling sites allows their interpolation by kriging [54]. In addition, as expected, the geostatistical parameters are also indicative of correlation between soil variables once they have presented similar ESD, mostly of medium dependence. This was also observed by [48] when they applied geostatistical analysis to soil-erodibility-factor data and other soil variables.

Through the interpolation, the similarity between the USLE K-factor and the RUSLE K-factor is clear, as is their relation to the other soil variables. Observing the maps, it is

possible to reaffirm the relevance of the grain size distribution in the USLE K-factor and the RUSLE K-factor. Nevertheless, the RUSLE K-factor seems to be more faithful to the soils of Caatinga than the USLE K-factor does. This may be justified by the small concentration of SOM in this soil, which drops the values of the USLE K-factor. According to [70] the typical soils of Caatinga have low SOM content because of the low input of organic residues, so the soil behavior is strongly dependent on parent material through its texture and poorly related to organic matter. On the other hand, the RUSLE K-factor is more indicated to study the common sandy soils of Caatinga, which presents small amount of SOM content.

4.4. Spectral Reflectance Data and Prediction Model Testing

The spectral analysis also shows that particle size distribution is a major influence on the average reflectance spectra of the investigated soils, as previously observed [77,100]. An evaluation of soils with varying soil texture but the same content of organic matter and pH revealed that an increase in clay content results in a decrease in spectral reflectance in the Vis-NIR range [77]. The results of this study show that the DRS may be used to predict both the USLE K-factor and the RUSLE K-factor in sandy soils of Caatinga. In cases where the SOM concentration is low, better mathematical parameters for calibration and external validation can be provided by combining the visible range to the NIR, as indicated by [101], in particular the combination between the visible region of 400–780 nm and the NIR region of 1200–1800 nm [17,101].

The absorption bands (valleys) in the spectra near to 1400, 1900, and 2200 nm also reveal the role played by soil texture in these NIR wavelengths. The spectral behavior at 1400 and 1900 nm may be associated with 2:1 phyllosilicates, while the features at 1400 and 2200 nm may be associated with lattice OH [81,102]. In addition, the reflectance peaks around 2200 nm may also be due to the cation OH bonds in phyllosilicate minerals, SiOH bonds, and organic molecules (e.g., CH_2, CH_3, and NH_3) [24,103]. Other studies have also associated the features at these wavelengths to 2:1 phyllosilicates [104,105]. These 2:1 phyllosilicates are mostly expansive clays, which usually do not provide for well-structured soils, because of their swelling–shrinkage behavior.

The possible occurrence of expansive clays in the studied soils is further corroborated by the CDW rates, which suggests the low capacity of these soils to form aggregates [106], resulting in a higher susceptibility of soil to erosion [107]. The variations in reflectance intensity and the shapes of the spectral curves observed in this study are also associated with the high content of sand fraction. The presence of bright minerals, such as quartz and feldspar, leads to high reflectance [77,103], which increases with increasing particle size, as observed in this study. Consequently, this composition is also influencing the prediction of silt and both the USLE K-factor and the RUSLE K-factor.

4.5. Study Limitations and Future Work

Although the USLE and its revised forms have been widely used to predict soil loss in many studies throughout the world, the efficacy of this model is dependent on the accuracy of the K-factor as an input variable. However, because the equation used for predicting the K-factor was developed from rainfall simulation data that originated from medium-textured soils in a relatively wet, temperate region (the US Midwest), it may not be readily applicable to arid regions with markedly different soil conditions (like our study area). Others have reached similar conclusions, when applying the (R)USLE K-factors in arid regions elsewhere [13,49]. To address this issue, these authors developed updated soil-loss equations that consider the specific soil and climatic conditions of arid regions. These updated equations were also used in our study.

Like any model, there are uncertainties associated with soil erosion models that cannot account for all the complex interactions between local soils and their surrounding climate, topography, and land use. Hence, unless extensive parameterization and validation against observed data are accomplished, soil-loss rates from models should be taken as best available estimates instead of absolute values [8]. By testing the suitability of the (R)USLE

for the specific conditions of a tropical arid region, our study provides an additional data point on the applicability of soil erosion models for a wide range of conditions.

Future work will involve applying a similar approach to test the applicability (sensitivity analysis) of other input variables to modeling soil erosion in the semiarid Brazilian condition, in particular the rainfall erosivity factor (R-factor) and the slope-length and steepness factors (L- and S-factors). We also plan to compare some of the pedotransfer functions derived from different countries and regions and evaluate their suitability to the soil and climate conditions of our study area.

5. Conclusions

This study demonstrated that the variability of both the USLE K-factor and the RUSLE K-factor is determined mainly by the parent material of the soil of Caatinga because of the insignificant amount of SOM. As the SOM does not represent a parameter to obtain the RUSLE K-factor, it is presented as a model more indicated to study typical soils of Caatinga. The values of the USLE K-factor and the RUSLE K-factor increased as the content of the clay also increased, suggesting the predominance of expansive 2:1 phyllosilicates in the colloidal fraction. This research also revealed that sand, silt, clay, CS, MS, FS, the USLE K-factor, and the RUSLE K-factor have spatial dependence. The RUSLE K-factor changed abruptly with long distance, whereas the USLE K-factor changed irregularly over short distances.

The maps showed the similarity between the RUSLE K-factor and the RUSLE K-factor. However, the map of the RUSLE K-factor was more realistic because of its higher correspondence to the maps of the sand, silt, and clay. Moreover, it was illustrated that the DRS may be used to predict both the USLE K-factor and the RUSLE K-factor in the sandy soils of Caatinga. This prediction may be carried out through PLSR, using specters in the NIR. The main wavelengths to do so were near to 1400, 1900, and 2200 nm. As the NIR is more accurate to predict sand, silt, and clay than SOM, it is more indicated to predict the USLE K-factor than the RUSLE K-factor.

These conclusions are important to help society to promote sustainable land management in sandy soils in dry environments. The application of DRS to predict and map soil erodibility must be tested in other sandy soils in order to give more validity to its use worldwide. Eventually, governments could use this approach to improve the system of monitoring agricultural areas to prevent and control soil erosion. This monitoring can be adopted as a strategy of land management, which can be an important step to achieve soil and water conservation. This achievement is especially important in biomes that are naturally dry, such as Caatinga.

Author Contributions: Conceptualization, S.F.P. and R.S.B.; methodology, V.M. and R.S.B.; software, Y.J.A.B.d.S. and R.S.B.; validation, R.S.B. and V.M.; formal analysis, S.F.P. and C.L.B.; investigation, S.F.P. and R.S.B.; resources, J.S.D. and R.S.B.; data curation, S.F.P. and R.S.B.; writing—original draft preparation, S.F.P. and C.L.B.; writing—review and editing, S.F.P. and O.S.C.J.; visualization, A.S.F.A. and O.S.C.J.; supervision, Y.J.A.B.d.S. and R.S.B.; project administration, R.S.B. All authors have read and agreed to the published version of the manuscript.

Funding: This research received no external funding.

Data Availability Statement: Not applicable.

Acknowledgments: We thank the Federal University of Piauí/Campus Professora Cinobelina Elvas (UFPI/CPCE), the Agricultural Science Graduate Program (PPGCA), and the Coordination for the Improvement of Higher Education Personnel (CAPES) for providing the infrastructure and financial support for sampling and for soil analysis. We also thank the research group Pedology Applied to Environmental Sustainability for their support during this project. We also thank the Federal University of Campina Grande for the partnership.

Conflicts of Interest: The authors declare no conflict of interest.

References

1. Ou, X.; Hu, Y.; Li, X.; Guo, S.; Liu, B. Advancements and challenges in rill formation, morphology, measurement, and modeling. *Catena* **2021**, *196*, 104932. [CrossRef]
2. Amundson, R.; Berhe, A.A.; Hopmans, J.W.; Olson, C.; Sztein, A.E.; Sparks, D.L. Soil and human security in the 21st century. *Science* **2015**, *348*, 1261071. [CrossRef] [PubMed]
3. Bullock, P. Climate Change Impacts. In *Encyclopedia of Soils in the Environment*; Elsevier: Amsterdam, The Netherlands, 2005; pp. 254–262.
4. Ozsahin, E.; Duru, U.; Eroglu, I. Land Use and Land Cover Changes (LULCC), a Key to Understand Soil Erosion Intensities in the Maritsa Basin. *Water* **2018**, *10*, 335. [CrossRef]
5. Salehi-Varnousfaderani, B.; Honarbakhsh, A.; Tahmoures, M.; Akbari, M. Soil erodibility prediction by Vis-NIR spectra and environmental covariates coupled with GIS, regression and PLSR in a watershed scale, Iran. *Geoderma Reg.* **2022**, *28*, e00470. [CrossRef]
6. Ostovari, Y.; Ghorbani-Dashtaki, S.; Kumar, L.; Shabani, F. Soil erodibility and its prediction in semi-arid regions. *Arch. Agron. Soil Sci.* **2019**, *65*, 1688–1703. [CrossRef]
7. Wadoux, A.M.J.C.; Odeh, I.O.A.; McBratney, A.B. Overview of Pedometrics. In *Reference Module in Earth Systems and Environmental Sciences*; Elsevier: Amsterdam, The Netherlands, 2021. [CrossRef]
8. Wischmeier, W.H.; Smith, D.D. *Predicting Rainfall Erosion Losses: A Guide to Conservation Planning*; Agriculture Handbook #537; US Department of Agriculture, Government Printing Office: Washington, DC, USA, 1978; p. 58.
9. Renard, K.G.; Foster, G.A.; Weesies, G.A.; MccooL, D.K. *Predicting Soil Erosion by Water: A Guide to Conservation Planning with the Revised Universal Soil Loss Equation (RUSLE)*; Agriculture Handbook #703; US Department of Agriculture, Government Printing Office: Washington, DC, USA, 1997; p. 407.
10. Kamel, T.A.; Achite, M.; Ouillon, S.; Dehni, A. Soil erodibility mapping using the RUSLE model to prioritize erosion control in the Wadi Sahouat basin, North-West of Algeria. *Environ. Monit. Assess.* **2018**, *1*, 190. [CrossRef]
11. Jiang, Q.; Chen, Y.; Hu, J.; Liu, F. Use of Visible and Near-Infrared Reflectance Spectroscopy Models to Determine Soil Erodibility Factor (K) in an Ecologically Restored Watershed. *Remote Sens.* **2020**, *12*, 3103. [CrossRef]
12. Wang, G.; Wu, B.; Zhang, L.; Jiang, H.; Xu, Z. Role of soil erodibility in affecting available nitrogen and phosphorus losses under simulated rainfall. *J. Hydrol.* **2014**, *514*, 180–191. [CrossRef]
13. Shabani, F.; Kumar, L.; Esmaeili, A. Improvement to the prediction of the USLE K-factor. *Geomorphology* **2014**, *204*, 229–234. [CrossRef]
14. Lal, R. (Ed.) *Soil Erosion Research Methods*, 2nd ed.; CRC-St. Lucie Press: Delray Beach, FL, USA, 1994; p. 352.
15. Coblinski, J.A.; Giasson, É.; Demattê, J.A.M.; Dotto, A.C.; Costa, J.J.F.; Vašát, R. Prediction of soil texture classes through different wavelength regions of reflectance spectroscopy at various soil depths. *Catena* **2020**, *189*, 104485. [CrossRef]
16. Naimi, S.; Ayoubi, S.; Di Raimo, L.A.D.L.; Dematte, J.A.M. Quantification of some intrinsic soil properties using proximal sensing in arid lands: Application of Vis-NIR, MIR, and pXRF spectroscopy. *Geoderma Reg.* **2022**, *28*, e00484. [CrossRef]
17. Viscarra Rossel, R.A.; Walvoort, D.J.J.; McBratney, A.B.; Janik, L.J.; Skjemstad, J.O. Visible, near infrared, mid infrared or combined diffuse reflectance spectroscopy for simultaneous assessment of various soil properties. *Geoderma* **2006**, *131*, 59–75. [CrossRef]
18. Wang, S.; Li, W.; Li, J.; Liu, X. Prediction of soil texture using FT-NIR Spectroscopy and PXRF Spectrometry with Data Fusion. *Soil Sci.* **2014**, *178*, 626–638. [CrossRef]
19. Zhu, Y.; Weindorf, D.C.; Zhang, W. Characterizing soils using a portable X-ray fluorescence spectrometer: 1. Soil texture. *Geoderma* **2011**, *167–168*, 167–177. [CrossRef]
20. Wang, L.; Cheng, Y.; Lamb, D.; Naidu, R. The application of rapid handheld FTIR petroleum hydrocarbon-contaminant measurement with transport models for site assessment: A case study. *Geoderma* **2020**, *361*, 114017. [CrossRef]
21. McClure, W.F. 204 years of near infrared technology: 1800–2003. *J. Near Infrared Spectrosc.* **2003**, *11*, 487–518. [CrossRef]
22. Pasquini, C. Near infrared spectroscopy: A mature analytical technique with new perspectives—A review. *Anal. Chim. Acta* **2018**, *1026*, 8–36. [CrossRef]
23. Workman, J.J., Jr. Interpretive spectroscopy for near infrared. *Appl. Spectrosc. Rev.* **1996**, *31*, 251–320. [CrossRef]
24. Clark, R.N.; King, T.V.V.; Klejwa, M.; Swayze, G.A. High spectral resolution reflectance spectroscopy of minerals. *J. Geophys. Res.* **1990**, *95*, 653–680. [CrossRef]
25. Nguyen, T.T.; Janik, L.J.; Raupach, M. Diffuse reflectance infrared Fourier transform (DRIFT) spectroscopy in soil studies. *Aust. J. Soil Res.* **1991**, *29*, 49–67. [CrossRef]
26. Viscarra Rossel, R.A.; Hicks, W.S. Soil carbon and its fractions estimated by visible near infrared transfer functions. *Eur. J. Soil Sci.* **2015**, *66*, 438–450. [CrossRef]
27. Viscarra-Rossel, R.A.; Behrens, T.; Ben-Dor, E.; Chabrillat, S.; Dematte, J.A.M.; Ge, Y.; Gomez, C.; Guerrero, C.; Peng, Y.; Ramirez-Lopez, L.; et al. Diffuse reflectance spectroscopy for estimating soil properties: A technology for the 21st century. *Eur. J. Soil Sci.* **2022**, *73*, e13271. [CrossRef]
28. Sampaio, E.V.S.B. Overview of the Brazilian caatinga. In *Seasonally Dry Tropical Forests*; Bullock, S.H., Mooney, H.A., Medina, E., Eds.; Cambridge University Press: New York, NY, USA, 1995; Volume 1, pp. 35–63.
29. Menezes, R.S.C.; Sampaio, E.V.S.B.; Giongo, V.; Pérez-Marin, A.M. Biogeochemical cycling in terrestrial ecosystems of the Caatinga Biome. *Braz. J. Biol.* **2012**, *72*, 643–653. [CrossRef] [PubMed]

30. Silva, J.M.C.; Leal, I.R.; Tabarelli, M. *Caatinga: The Largest Tropical Dry Forest Region in South America*; Springer: Berlin/Heidelberg, Germany, 2017; pp. 1–482.
31. Silva, F.B.R.; Riche, G.R.; Tonneau, J.P.; Souza Neto, N.C.; Brito, L.T.L.; Correia, R.C.; Cavalcante, A.C.; Silva, A.B.; Araujo Filho, J.C.; Leite, A.P. *Northeast Agro-Ecological Zoning: Diagnosis of the Natural and Agro-Socio-Economic Framework*; EMBRAPA-CPATSA: Petrolina, Brazil, 1993; p. 325.
32. Queiroz, L.P.; Cardoso, D.; Fernandes, M.F.; Moro, M.F. Diversity and evolution of flowering plants of the Caatinga domain. In *Caatinga: The Largest Tropical Dry Forest Region in South America*; Silva, J.M.C., Leal, I.R., Tabarelli, M., Eds.; Springer: Cham, Switzerland, 2017; pp. 23–63.
33. Medeiros, S.S.; Cavalcante, A.M.B.; Marin, A.M.P.; Tinoco, L.B.M.; Salcedo, I.H.; Pinto, T.F. *Synopsis of the Demographic Census for the Brazilian Semiarid Region*; Semiarid National Institute (INSA): Campina Grande, Brazil, 2012; pp. 1–107.
34. Araújo Filho, J.C. *Manejo Pastoril Sustentável da Caatinga*; Projeto Dom Helder Camara: Recife, Brasil, 2013; pp. 1–200.
35. Palacio, H.A.Q.; Ribeiro Filho, J.C.; Santos, J.C.N.; Andrade, E.M.; Brasil, J.B. Effective precipitation, soil loss, and plant cover systems in the Caating biome, Brazil. Rev. *Caatinga* **2016**, *29*, 956–965. [CrossRef]
36. Tomasella, J.; Vieira, R.M.S.P.; Barbosa, A.A.; Rodriguez, D.A.; Santana, M.O.; Sestini, M.F. Desertification trends in the Northeast of Brazil over the period 2000–2016. *Int. J. Appl. Earth Obs. Geoinf.* **2018**, *73*, 197–206. [CrossRef]
37. Borrelli, P.; Robinson, D.A.; Fleischer, L.R.; Lugato, E.; Ballabio, C.; Alewell, C.; Meusburger, K.; Modugno, S.; Schütt, B.; Ferro, V.; et al. An assessment of the global impact of 21st century land use change on soil erosion. *Nat. Commun.* **2017**, *8*, 2013. [CrossRef]
38. Rodrigues, L.U.; Silva, R.R. Boron Availability in Building up Fertility in Cerrado Soil of Tocantins. *Commun. Soil Sci. Plant Anal.* **2020**, *51*, 595–603. [CrossRef]
39. Lopes, A.A.C.; Bogiani, J.C.; Figueiredo, C.C.; Junior, F.B.R.; Sousa, D.M.G.; Malaquias, J.V.; Mendes, I.C. Enzyme activities in a sandy soil of Western Bahia under cotton production systems: Short-term effects, temporal variability, and the FERTBIO sample concept. *Braz. J. Microbiol.* **2021**, *52*, 2193–2204. [CrossRef]
40. Alvares, A.A.; Stape, J.L.; Sentelhas, P.C.; Goncalves, J.L.M.; Sparovek, G. Koppen's climate classification map for Brazil. *Meteorol. Z.* **2014**, *22*, 711–728. [CrossRef]
41. Torres, F.S.M.; Silva, E.P. *Geodiversity of the Paraíba State*; CPRM: Recife, Brazil, 2016.
42. Santos, H.G.; Jacomine, P.K.T.; Anjos, L.H.C.; Oliveira, V.A.; Lumbreras, J.F.; Coelho, M.R.; Almeida, J.A.; Araújo Filho, J.C.; Oliveira, J.B.; Cunha, T.J.F. *Brazilian Soil Classification System*, 5th ed.; Revised and Extended; Embrapa: Brasília, Brazil, 2018.
43. IUSS Working Group WRB. *World Reference Base for Soil Resources. International Soil Classification System for Naming Soils and Creating Legends for Soil Maps*, 4th ed.; International Union of Soil Sciences (IUSS): Vienna, Austria, 2022.
44. Soil Survey Staff. *Soil Taxonomy: A Basic System of Soil Classification for Making and Interpreting Soil Surveys*, 2nd ed.; Handbook 436; Natural Resources Conservation Service, U.S. Department of Agriculture: Washington, DC, USA, 1999.
45. Leprun, J.C. *Report on the End of the Soil Management and Conservation Agreement in Northeast Brazil (1982–1983)*; SUDENE: Recife, Brazil, 1983; p. 290.
46. Teixeira, P.C.; Donagemma, G.K.; Fontana, A.; Teixeira, W.G. *Manual of Soil Analysis Methods*, 3rd ed.; Embrapa: Brasilia, Brazil, 2017.
47. Van Raij, B.; Andrade, J.C.; Cantarella, H.; Quaggio, J.A. (Eds.) Determination of Organic Matter. In *Chemical Analysis for Tropical Soils Fertility Evaluation*; Agronomical Institute of Campinas: Campinas, Brasil, 2001; Volume 1.
48. Barbosa, R.S.; Marques, J.R.J.; Barrón, V.; Martins Filho, M.V.; Siqueira, D.S.; Peluco, R.G.; Camargo, L.A.; Silva, L.S. Prediction and mapping of erodibility factors (USLE and WEPP) by magnetic susceptibility in basalt-derived soils in northeastern São Paulo state, Brazil. *Environ. Earth Sci.* **2019**, *78*, 1–12. [CrossRef]
49. Ostovari, Y.; Ghorbani-Dashtaki, S.; Bahrami, H.-A.; Naderi, M.; Dematthê, J.A.M.; Kerry, R. Modification of the USLE K factor for soil erodibility assessment on calcareous soils in Iran. *Geomorphology* **2016**, *273*, 385–395. [CrossRef]
50. Denardin, J.E. Soil Erodibility Estimated by Physical and Chemical Parameters. Ph.D. Thesis, Luis de Queiroz College of Agriculture, University of São Paulo, Piracicaba, Brazil, 1990.
51. Wischmeier, W.H.; Johnson, C.B.; Cross, B.V. A Soil Erodibility Nomograph for Farmland and Construction Sites. *J. Soil Water Conserv.* **1971**, *26*, 189–193.
52. Camargo, L.A.; Marques Júnior, J.; Barrón, V.; Alleoni, L.R.F.; Barbosa, R.S.; Pereira, G.T. Mapping of clay, iron oxide and adsorbed phosphate in Oxisols using diffuse reflectance spectroscopy. *Geoderma* **2015**, *251–252*, 124–132. [CrossRef]
53. Oliveira, R.P.; Barbosa, R.S.; Marques Júnior, J.; Silva, Y.J.A.B.; Barrón, V.; Dantas, J.S.; Resende, J.M.A.; Gualberto, A.V.S. Mid-Infrared Spectrum Analysis for Mapping Attributes of Cohesive Soils in Brazil. *Commun. Soil Sci. Plant Anal.* **2022**, *53*, 1277–1293. [CrossRef]
54. Vieira, S.R. Geostatistics use in studies of spatial variability of soil properties. In *Topics in Soil Science*; Novais, R.F., Alvarez, V.V.H., Schaefer, C.E.G.R., Eds.; Brazilian Society of Soil Science: Viçosa, Brasil, 2000; Volume 1, pp. 1–54.
55. Cambardella, C.A.; Moorman, T.B.; Novak, J.M.; Parkin, T.B.; Karlen, D.L.; Turco, R.F.; Konopa, A.E. Field-scale variability of soil properties in central Iowa soils. *Soil Sci. Soc. Am. J.* **1994**, *58*, 1501–1511. [CrossRef]
56. Geladi, P.; Kowalski, B.R. Partial least-squares regression: A tutorial. *Anal. Chim. Acta* **1986**, *185*, 1–17. [CrossRef]
57. Viscarra-Rossel, R.A. ParLeS: Software for chemometric analysis of spectroscopic data. *Chemom. Intell. Lab. Syst.* **2008**, *90*, 72–83. [CrossRef]

58. Efron, B.; Tibshirani, R.F. *An Introduction to the Bootstrap*; Chapman & Hall: London, UK, 1993.
59. Akaike, H. Information theory as an extension of the maximum likelihood principle. In Proceedings of the 2nd International Symposium on Information Theory, Tsahkadsor, Armenia, USSR, 2–8 September 1971; Akadêmia Kiadó: Budapest, Hungary, 1973; pp. 267–281.
60. Tabatabai, S.; Knadel, M.; Thomsen, A.; Greve, M.H. On-the-Go Sensor Fusion for Prediction of Clay and Organic Carbon Using Pre-processing Survey, Different Validation Methods, and Variable Selection. *Am. J. Soil Sci.* **2019**, *83*, 300–310. [CrossRef]
61. Ng, W.; Minasny, B.; Mendes, W.S.; Demattê, J.A.M. The influence of training sample size on the accuracy of deep learning models for the prediction of soil properties with near-infrared spectroscopy data. *Soil* **2020**, *6*, 565–578. [CrossRef]
62. Cezar, E.; Nanni, M.R.; Crusiol, L.G.T.; Sun, L.; Chicati, M.S.; Furlanetto, R.H.; Rodrigues, M.; Sibaldelli, R.N.R.; Silva, G.F.C.; Oliveira, K.M.; et al. Mapping Particle Size and Soil Organic Matter in Tropical Soil Based on Hyperspectral Imaging and Non-Imaging Sensors. *Remote Sens.* **2021**, *13*, 1376. [CrossRef]
63. Dhawale, N.M.; Adamchuk, V.I.; Prasher, S.O.; Viscarra Rossel, R.A. Evaluating the Precision and Accuracy of Proximal Soil vis–NIR Sensors for Estimating Soil Organic Matter and Texture. *Soil Syst.* **2021**, *5*, 48. [CrossRef]
64. Zhou, P.; Sudduth, K.A.; Veum, K.S.; Li, M. Extraction of reflectance spectra features for estimation of surface, subsurface, and profile soil properties. *Comput. Electron. Agric.* **2022**, *196*, 106845. [CrossRef]
65. Chang, C.W.; Laird, D.; Mausbach, M.J.; Hurburgh, C.R. Near-Infrared Reflectance Spectroscopy–Principal Components Regression Analyses of Soil Properties. *Soil Sci. Soc. Am. J.* **2001**, *65*, 480–490. [CrossRef]
66. Yan, B.; Fang, N.F.; Zhang, P.C.; Shi, Z.H. Impacts of land use change on watershed streamflow and sediment yield: An assessment using hydrologic modelling and partial least squares regression. *J. Hydrol.* **2013**, *484*, 26–37. [CrossRef]
67. Salviano, A.M.; Cunha, T.J.F.; Olszevski, N.; Oliveira Neto, M.B.; Giongo, V.; Queiroz, A.F.; Menezes, F.J.S. Potentialities and limitations for the agricultural use of sandy soils in the semiarid region of Bahia. *Magistra* **2016**, *28*, 137–148.
68. Santos, E.S.; Souza, E.S.; Pessoa, L.G.M.; Leite, P.A.; Wilcox, B.P.; Silva, J.R.I. Water erosion in Caatinga and degraded pasture areas in semiarid region. *Amazon. J. Plant Res.* **2018**, *2*, 261–266. [CrossRef]
69. Souza, J.J.L.L.; Souza, B.I.; Xavier, R.A.; Cardoso, E.C.M.; Medeiros, J.R.; Fonseca, C.F.; Schaefer, C.E.G.R. Organic carbon rich-soils in the Brazilian semiarid region and paleoenvironmental implications. *Catena* **2022**, *212*, 106101. [CrossRef]
70. Araújo Filho, J.C.; Ribeiro, M.R.; Burgos, N.; Marques, F.A. Solos da Caatinga. In *Pedology—Soils of the Brazilian Biomes*; Curi, N., Ker, J.C., Novais, R.F., Vidal-Torrado, P., Schaefe, C.E.G.R., Eds.; Brazilian Society of Soil Science: Viçosa, Brasil, 2017; Volume 1, pp. 227–260.
71. da Silva, R.J.A.B.; da Silva, Y.J.A.B.; van Straaten, P.; do Nascimento, C.W.A.; Biondi, C.M.; da Silva, Y.J.A.B.; Araújo Filho, J.C. Influence of parent material on soil chemical characteristics in a semi-arid tropical region of Northeast Brazil. *Environ. Monit. Assess.* **2022**, *194*, 1–21. [CrossRef]
72. Ostovari, Y.; Moosavi, A.A.; Mozaffari, H.; Poppiel, R.R.; Tayebi, M.; Dematte, J.A.M. Chapter 32—Soil erodibility and its influential factors in the Middle East. *Comput. Earth Environ. Sci.* **2022**, *1*, 441–454. [CrossRef]
73. Schmid, T.; Palacios-Orueta, A.; Chabrillat, S.; Bendor, E.; Plaza, A.; Rodriguez, M.; Huesca, M.; Pelayo, M.; Pascual, C.; Escribano, P.; et al. Spectral characteristic of land surface composition to determination soil erosion within semiarid ranifed cultivated areas. In Proceedings of the 2012 IEEE International Geoscience and Remote Sensing Symposium, Munich, Germany, 22–27 July 2012.
74. Lin, C.; Zhou, S.L.; Wu, S.H. Using hyperspectral reflectance to detect different soil erosion status in the Subtropical Hilly Region of Southern China: A case study of Changting, Fujian Province. *Environ. Earth Sci.* **2013**, *70*, 1661–1670. [CrossRef]
75. Guerra, A. The effect of organic matter content on soil erosion in simulated rainfall experiments in W. Sussex, UK. *Soil Use Manag.* **1994**, *10*, 60–64. [CrossRef]
76. Kuhn, N.J. Erodibility of soil and organic matter: Independence of organic matter resistance to interrill erosion. *Earth Surf. Process. Landf.* **2007**, *32*, 794–802. [CrossRef]
77. Ostovari, Y.; Ghorbani-Dashtaki, S.; Bahrami, H.A.; Abbasi, M.; Dematte, A.A.M.; Emmanuel, A.; Panagos, P. Towards prediction of soil erodibility, SOM and CaCO3 using Laboratory Vis NIR spectra: A case study in a semi-arid region of Iran. *Geoderma* **2018**, *314*, 102–112. [CrossRef]
78. Yost, J.L.; Hartemink, A.E. Chapter Four—Soil organic carbon in sandy soils: A review. *Adv. Agron.* **2019**, *158*, 217–310. [CrossRef]
79. Plante, A.F.; Conant, R.T.; Stewart, C.E.; Paustian, K.; Six, J. Impact of Soil Texture on the Distribution of Soil Organic Matter in Physical and Chemical Fractions. *Soil Sci. Soc. Am. J.* **2006**, *70*, 287–296. [CrossRef]
80. Marafon, G.; Barbosa, R.S.; Lacerda, J.J.J.; Martins, V.; Silva, J.D.F.; Costa, O.S., Jr. C and P pool restoration by a no-tillage system on Brazilian Cerrado Oxisol in Piauí State. *Environ. Monit. Assess.* **2020**, *192*, 254. [CrossRef]
81. Mendes, W.S.; Boechat, C.L.; Gualberto, A.V.S.; Barbosa, R.S.; Silva, Y.J.A.B.; Saraiva, P.C.; Sena, A.F.S.; Duarte, L.S.L. Soil spectral library of Piauí State using machine learning for laboratory analysis in Northeastern Brazil. *Rev. Braz. Ciênc. Solo* **2021**, *45*, e0200115. [CrossRef]
82. Adhikari, G.; Bhattacharyya, K.G. Correlation of soil organic carbon and nutrients (NPK) to soil mineralogy, texture, aggregation, and land use pattern. *Environ. Monit. Assess.* **2015**, *187*, 1–18. [CrossRef]
83. Songu, G.A.; Abu, R.D.; Temwa, N.M.; Yiye, S.T.; Wahab, S.; Mohammed, B.G. Analysis of Soil Erodibility Factor for Hydrologic Processes in Kereke Watershed, North Central Nigeria. *J. App. Sci. Environ. Manag.* **2021**, *25*, 425–432. [CrossRef]

84. Chen, S.; Zhang, G.; Zhu, P.; Wang, C.; Wan, Y. Impact of slope position on soil erodibility indicators in rolling hill regions of northeast China. *Catena* **2022**, *217*, 106475. [CrossRef]
85. Olaniya, M.; Bora, P.K.; Das, S.; Chanu, P.H. Soil erodibility indices under different land uses in Ri-Bhoi district of Meghalaya (India). *Sci. Rep.* **2020**, *10*, 14986. [CrossRef] [PubMed]
86. Santos, J.C.N.; Andrade, E.M.; Medeiros, P.H.A.; Guerreiro, M.J.S.; Palacio, H.A.Q. Land use impact on soil erosion at different scales in the Brazilian semi-arid. *Rev. Ciênc. Agron.* **2017**, *48*, 251–260. [CrossRef]
87. Lei, W.; Dong, H.; Chen, P.; Lv, H.; Fan, L.; Mei, G. Study on Runoff and Infiltration for Expansive Soil Slopes in Simulated Rainfall. *Water* **2020**, *12*, 222. [CrossRef]
88. Han, D.D.; Deng, J.C.; Gu, C.J.; Mu, X.M.; Gao, P.; Gao, J.J. Effect of shrub-grass vegetation coverage and slope gradient on runoff and sediment yield under simulated rainfall. *Int. J. Sediment Res.* **2020**, *36*, 29–37. [CrossRef]
89. Li, C.J.; Pan, C.Z. Overland runoff erosion dynamics on steep slopes with forages under field simulated rainfall and inflow. *Hydrol. Process.* **2020**, *34*, 1794–1809. [CrossRef]
90. Sampaio, E.V.S.B.; Menezes, R.S.C. Perspectives of the land use in the northeastern semi-arid region. In *500 Years of Soil Use in Brazil*; Araújo, Q.R., Ed.; Brazilian Society of Soil Science: Viçosa, Brazil, 2002; pp. 339–363.
91. Sampaio, E.V.S.B.; Araújo, M.S.B.; Salcedo, I.H.; Menezes, R.S.C. *Sustainable Management of the Northeastern Semiarid Region*; University Press: Recife, Brazil, 2009; p. 149.
92. Espindola, G.M.; Figueredo, E.S.; Picanço Júnior, P.; dos Reis Filho, A.A. Cropland expansion as a driver of land-use change: The case of Cerrado-Caatinga transition zone in Brazil. *Environ. Dev. Sustain* **2021**, *23*, 17146–17160. [CrossRef]
93. Brazilian Agricultural Research Corporation. Caatinga Biome. Strategic Territorial Intelligence System. Available online: https://www.embrapa.br/bioma-caatinga (accessed on 14 November 2022).
94. Oliveira, G.F.; Garcia, A.C.L.; Montes, M.A.; Jucá, J.C.L.D.A.; Valente, V.L.D.S.; Rohde, C. Are conservation units in the Caatinga biome, Brazil, efficient in the protection of biodiversity? An analysis based on the drosophilid fauna. *J. Nat. Conserv.* **2016**, *34*, 145–150. [CrossRef]
95. Addis, H.K.; Klik, A. Predicting the spatial distribution of soil erodibility factor using USLE nomograph in an agricultural watershed, Ethiopia. *Int. Soil Water Conserv. Res.* **2015**, *3*, 282–290. [CrossRef]
96. Panagos, P.; Meusburger, K.; Ballabio, C.; Borrelli, P.; Alewell, C. Soil erodibility in Europe: A high-resolution dataset based on LUCAS. *Sci. Total Environ.* **2014**, *479–480*, 189–200. [CrossRef]
97. Bonilla, C.A.; Johnson, O. Soil erodibility mapping and its correlation with soil properties in Central Chile. *Geoderma* **2012**, *189–190*, 116–123. [CrossRef]
98. Montanari, R.; Zambianco, E.C.; Corrêa, A.R.; Pellin, D.M.P.; Carvalho, M.P.; Dalchiavon, F.C. Physical attributes of an Oxisol linear and spatially correlated with millet + pigeonpea intercropping. *Rev. Ceres* **2012**, *59*, 125–135. [CrossRef]
99. Vaezi, A.R.; Hasanzadeh, H.; Cerdà, A. Developing an erodibility triangle for soil textures in semi-arid regions, NW Iran. *Catena* **2016**, *142*, 221–232. [CrossRef]
100. Viscarra-Rossel, R.A. Robust modelling of soil diffuse reflectance spectra by "bagging-partial least squares regression". *J. Near Infrared Spectrosc.* **2007**, *15*, 37–47. [CrossRef]
101. Xu, L.; Hong, Y.; Wei, Y.; Guo, L.; Shi, T.; Liu, Y.; Jiang, Q.; Fei, T.; Liu, Y.; Mouazen, A.M.; et al. Estimation of Organic Carbon in Anthropogenic Soil by VIS-NIR Spectroscopy: Effect of Variable Selection. *Remote Sens.* **2020**, *12*, 3394. [CrossRef]
102. Viscarra-Rossel, R.A.; Behrens, T.; Ben-Dor, E.; Brown, D.J.; Demattê, J.A.M.; Shepherd, K.D.; Shi, Z.; Stenberg, B.; Stevens, A.; Adamchuk, V.; et al. A global spectral library to characterize the world's soil. *Earth Sci Rev.* **2016**, *155*, 198–230. [CrossRef]
103. Conforti, M.; Froio, R.; Matteucci, G.; Buttafuoco, G. Visible and near infrared spectroscopy for predicting texture in forest soil: An application in southern Italy. *Iforest-Biogeosci. For.* **2015**, *8*, 339–347. [CrossRef]
104. Demattê, J.A.M.; Horák-Terra, I.; Beirigo, R.M.; Terra, F.S.; Marques, K.P.P.; Fongaro, C.T.; Silva, A.C.; Vidal-Torrado, P. Genesis and properties of wetland soils by VIS-NIR-SWIR as a technique for environmental monitoring. *J. Environ. Manag.* **2017**, *197*, 50–62. [CrossRef]
105. Di Iorio, E.; Circelli, L.; Lorenzetti, R.; Costantini, E.A.C.; Egendorf, S.P.; Colombo, C. Estimation of andic properties from Vis-NIR diffuse reflectance spectroscopy for volcanic soil classification. *Catena* **2019**, *182*, 104109–104122. [CrossRef]
106. Santos, L.N.S.; Passos, R.R.; Silva, L.V.M.; Oliveira, P.P.; Garcia, G.O.; Cecílio, R.A. Evaluation of some physical attributes of an Oxisol under different crop cover. *Biosci. J.* **2010**, *26*, 940–947.
107. Santos, T.E.M.; Montenegro, A.A.A.; Silva Junior, V.P. Water erosion and organic carbon loss in different types of land cover in the semi-arid region, under simulated rainfall conditions. *Rev. Braz. Recur. Hídr.* **2008**, *13*, 113–125. [CrossRef]